The Astronomical Journal, 131:1090–1105, 2006 February

PLANETS IN STELLAR CLUSTERS EXTENSIVE SEARCH. IV. A DETECTION OF A POSSIBLE TRANSITING PLANET CANDIDATE IN THE OPEN CLUSTER NGC 2158[1]

B. J. Mochejska[2]
Department of Physics, Purdue University, 525 Northwestern Avenue, West Lafayette, IN 47907; bmochejs@cfa.harvard.edu

K. Z. Stanek
Department of Astronomy, The Ohio State University, 140 West 18th Avenue, Columbus, OH 43210;
kstanek@astronomy.ohio-state.edu

and

D. D. Sasselov, A. H. Szentgyorgyi, E. Adams, R. L. Cooper, J. B. Foster, J. D. Hartman,
R. C. Hickox, K. Lai, M. Westover, and J. N. Winn[2]
Harvard-Smithsonian Center for Astrophysics, 60 Garden Street, Cambridge, MA 02138; sasselov@cfa.harvard.edu, saint@cfa.harvard.edu,
era@improbable.org, rcooper@cfa.harvard.edu, jfoster@cfa.harvard.edu, jhartman@cfa.harvard.edu, rhickox@cfa.harvard.edu,
klai@cfa.harvard.edu, mwestover@cfa.harvard.edu, jwinn@cfa.harvard.edu
Received 2005 September 30; accepted 2005 October 27

ABSTRACT

We have undertaken a long-term project, Planets in Stellar Clusters Extensive Search, to search for transiting planets in open clusters. In this paper we present the results for NGC 2158, an intermediate-age, populous cluster. We have monitored the cluster for over 260 hours, spread over 59 nights. We have detected one candidate transiting low-luminosity object, with an eclipse depth of 3.7% in the *R* band. If the host star is a member of the cluster, the eclipse depth is consistent with a $1.7R_J$ object. Cluster membership of the host is supported by its location on the cluster main sequence and its close proximity to the cluster center (2′). We have discovered two other stars exhibiting low-amplitude (4%–5%) transits, V64 and V70, but they are most likely blends or field stars. Given the photometric precision and temporal coverage of our observations and the current best estimates for the frequency and radii of short-period planets, the expected number of detectable transiting planets in our sample is 0.13. We have observed four outbursts for the candidate cataclysmic variable V57. We have discovered 40 new variable stars in the cluster, bringing the total number of identified variables to 97, and present for them high-precision light curves, spanning 13 months.

Key words: binaries: eclipsing — novae, cataclysmic variables — planetary systems — stars: variables: other

1. INTRODUCTION

We have undertaken a long-term project, Planets in Stellar Clusters Extensive Search (PISCES), to search for transiting planets in open clusters. To date we have published a feasibility study based on one season of data for NGC 6791 (Mochejska et al. 2002, hereafter Paper I) and a catalog of 57 variable stars for our second target, NGC 2158, based on the data from the first observing season (Mochejska et al. 2004, hereafter Paper II). We have also published the results of an extensive search for transiting planets in NGC 6791, based on over 300 hr observations, spread over 84 nights (Mochejska et al. 2005, hereafter Paper III). We have not detected any promising candidates and have derived an estimate of 1.7 expected transiting planets.

In this paper we present the results of a search for transiting planets in the open cluster NGC 2158 $[(\alpha,\ \delta)_{2000} = (6^h7^m,\ +24^\circ0'); (l,\ b) = (186\overset{\circ}{.}63,\ +1\overset{\circ}{.}78)]$. It is a very populous, intermediate-age ($\tau = 2$–3 Gyr), rather metal-poor ([Fe/H] $= -0.46$) open cluster, located at a distance of 3.6 kpc (Carraro et al. 2002, hereafter Ca02; Christian et al. 1985).

Searching for planets in open clusters eliminates the problem of false detections due to blended eclipsing binary stars, which are a significant contaminant in the Galactic field searches (over 90% of all candidates; Konacki et al. 2003; Udalski et al. 2002b, 2002c). Blending causes a large decrease in the depth of the eclipses and mimics the transit of a much smaller object, such as a planet. As opposed to dense star fields in the disk of our Galaxy, open clusters located away from the Galactic plane are sparse enough for blending to be negligible.

There are two key elements in a survey for transiting planets. The most commonly emphasized requirement is the high photometric precision, at the 1% level. The more often overlooked factor is the need for very extensive temporal coverage.

Extensive temporal coverage is important because even for planets with periods between 1 and 2 days, the fractional transit length is only ∼5% of the period, and it drops to ∼2% for periods of 2–10 days. During the remaining 95%–98% of the period, the system is photometrically indistinguishable from stars without transiting planets. To our best knowledge, PISCES is the most extensive search for transiting planets in open clusters in terms of temporal coverage with a 1 m telescope.

The paper is arranged as follows: § 2 describes the observations, § 3 summarizes the reduction procedure, § 4 outlines the search strategy for transiting planets, § 5 gives an estimate of the expected number of transiting planet detections, and § 6 contains the variable star catalog. Concluding remarks are found in § 7.

2. OBSERVATIONS

The data analyzed in this paper were obtained at the Fred Lawrence Whipple Observatory (FLWO) 1.2 m telescope using the 4Shooter CCD mosaic with four thinned, backside-illuminated, AR-coated Loral 2048[2] CCDs (A. H. Szentgyorgyi et al. 2006, in

[1] Based on data from the Fred Lawrence Whipple Observatory 1.2 m telescope.
[2] Hubble Fellow.

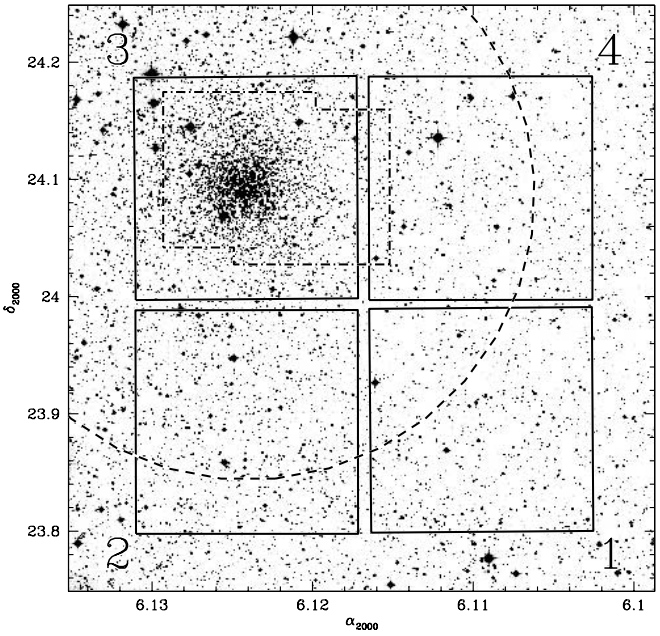

FIG. 1.—Digital Sky Survey image of NGC 2158 showing the field of view of the 4Shooter. The chips are numbered clockwise from 1 to 4 starting from the bottom right chip. NGC 2158 is centered on chip 3. North is up, and east is to the left.

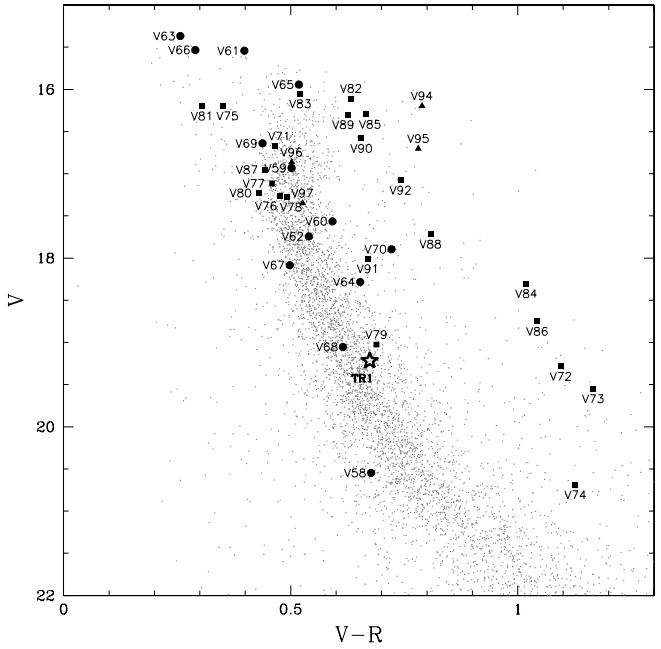

FIG. 2.—(V, $V-R$) CMD for chip 3, centered on NGC 2158. Newly discovered eclipsing binaries are plotted with circles, other periodic variables with squares, and the nonperiodic variables with triangles. The low-luminosity transiting object candidate, TR1, is plotted with a star.

preparation). The camera, with a pixel scale of 0.″33 pixel^{-1}, gives a field of view of 11.′4 × 11.′4 for each chip. The cluster was centered on chip 3 (Fig. 1). The data were collected during 59 nights, from 2003 January 3 to 2004 February 17. A total of 965 × 900 s R-band and 223 × 450 s V-band exposures were obtained.

3. DATA REDUCTION

3.1. *Image Subtraction Photometry*

The preliminary processing of the CCD frames was performed with the standard routines in the IRAF CCDPROC package.[3] Photometry was extracted using the ISIS image subtraction package (Alard & Lupton 1998; Alard 2000), as described in detail in Papers I and III.

The ISIS reduction procedure consists of the following steps: (1) transformation of all frames to a common (x, y) coordinate grid; (2) construction of a reference image from several of the best exposures; (3) subtraction of each frame from the reference image; (4) selection of stars to be photometered; and (5) extraction of profile photometry from the subtracted images.

We used the same parameters for image subtraction as in Paper III. The reference images were constructed from the 25 best exposures in the R and the best 12 in V.

3.2. *Calibration*

To calibrate the VR photometry we used two photometric catalogs: Ca02 and Kharchenko et al. 1997 (hereafter KAS97). The CCD photometry from Ca02 has higher accuracy, while the photographic catalog from KAS97 overlaps all four chips, but it has a different zero point and larger internal scatter, as described in Paper II.

The R-band photometry was calibrated from the photometry published by Ca02. We used 1685 stars above $R = 18.5$ to determine the zero point of the magnitude scale for chip 3. The rms scatter around the offset was 0.09. Offsets between chip 3 and the remaining chips were determined from an image, taken with chip 3, centered on the center of the array. The number of stars used to determine the offset was 121, 135, and 293 for chips 1, 2, and 4, respectively.

As a consistency check, we compared these offsets with those derived independently between chips 1 and 2 and KAS97, and chip 4 and Ca02. The differences in the offsets were 0.215, 0.181, and 0.010, based on 19, 90, and 36 stars, respectively. For chip 4, as expected, there is excellent agreement, while for chips 1 and 2 the different zero point of the two catalogs is apparent.

The V-band photometry for chips 1 and 2 was calibrated against KAS97. To determine the zero points we used 19 and 90 stars above 17 mag for chips 1 and 2, respectively. The rms scatter of the residuals was 0.13 on both chips.

The V-band photometry for chips 3 and 4 was calibrated against Ca02. The zero points were derived from 1554 and 36 stars above 19 and 20 mag, and the rms scatter of the residuals was 0.09 and 0.06, respectively. Figure 2 shows the calibrated (V, $V-R$) color-magnitude diagram (CMD) for the chip 3 reference image.

3.3. *Astrometry*

Equatorial coordinates were determined for the R-band reference image star lists. The transformation from rectangular to equatorial coordinates was derived using 596, 710, 1952, and 615 transformation stars from the 2MASS catalog (Cutri et al. 2003) in chips 1–4, respectively. The rms deviation between the catalog and the computed coordinates for the transformation stars was 0.″12 in right ascension and 0.″11 in declination.

4. SEARCH FOR TRANSITING PLANETS

4.1. *Further Data Processing*

We rejected from further analysis 96 R-band epochs in which fewer than 4000 stars were detected on chip 3 by DAOphot

[3] IRAF is distributed by the National Optical Astronomy Observatory, which is operated by the Association of Universities for Research in Astronomy, Inc., under cooperative agreement with the NSF.

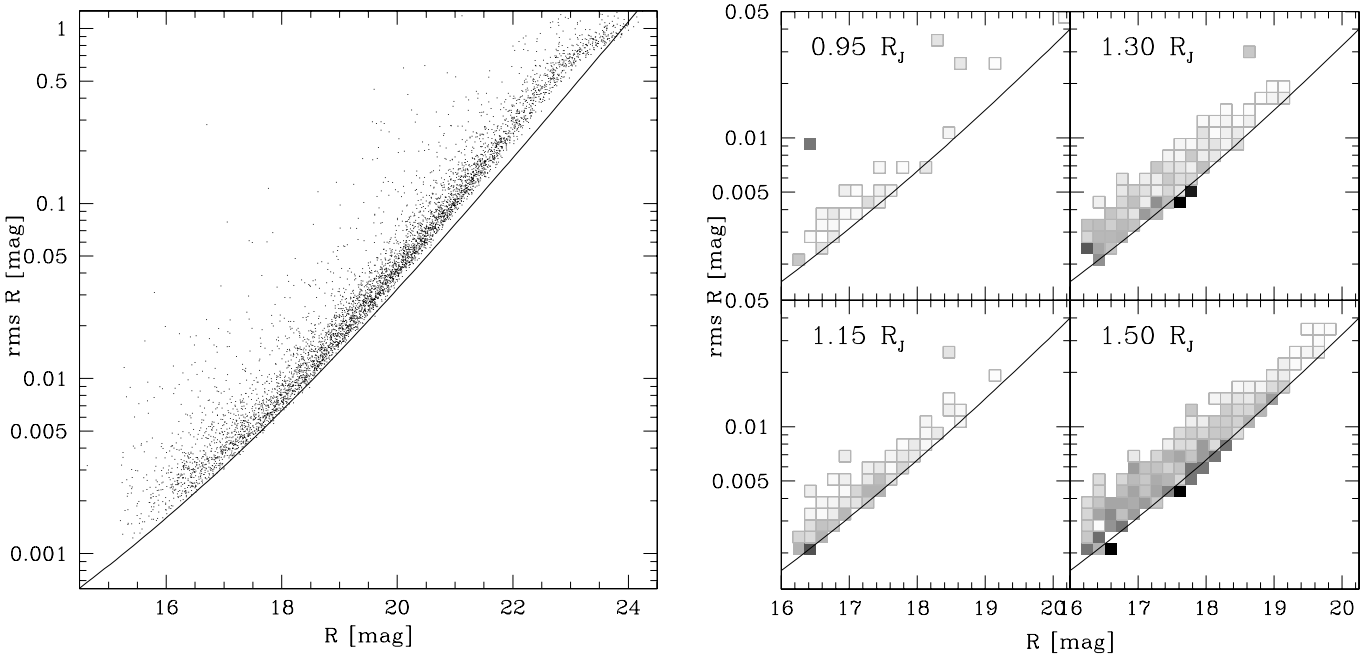

FIG. 3.—*Left*: The rms scatter of the *R*-band light curves for stars on chip 3 with at least 500 data points. The solid curve indicates the photometric precision limit due to Poisson noise of the star and average sky brightness. *Right*: Detection efficiency of 0.95, 1.15, 1.30, and 1.50R_J planets as a function of magnitude and rms scatter (*white*: 0%; *black* 100%), determined in § 5.2.

(Stetson 1987). We also rejected an additional 29–31 bad-quality images from four nights. For chip 3, which suffers from moderate crowding and contains a significant number of saturated stars, we also rejected an additional 78 epochs in which the FWHM of the stellar point-spread function (PSF) was greater than 10 pixels and the sky level was over 10,000 ADU. This left us with the 807, 809, 729, and 809 highest quality *R*-band exposures on chips 1–4, with a median seeing of 2.″3. We also removed 6 *V*-band images, which left us with 217 exposures with a median seeing of 2.″6.

In the NGC 6791 data, analyzed in Paper III, we noted in the light curves the presence of offsets between different runs. These were probably due to the periodic UV flooding of the CCD camera, which alters its quantum efficiency as a function of wavelength. In the NGC 2158 data set analyzed here, this problem was found to be much less prominent, possibly due to the fact that this data set was obtained over a shorter period of time (12.5 months, compared to 24 months for NGC 6791). To prevent the transit detection algorithm from mistaking these changes in brightness for transits, we corrected the light curves using the method proposed by Tamuz et al. (2005). This algorithm was originally envisioned to correct for color-dependent atmospheric extinction but can be used to correct for any linear systematic effects. We solve for coefficients c_i and a_j that minimize the following equation:

$$S_i^2 = \sum_j \frac{(r_{ij} - c_i a_j)^2}{\sigma_{ij}^2}, \quad (1)$$

where r_{ij} is the residual for the observation of the ith star on the jth image, or the star's average-subtracted magnitude, and σ_{ij} is the uncertainty of the measurement of star i on image j. Following Tamuz et al. (2005), the air masses were used as initial a_j-coefficients. We chose to run this algorithm four times. After the fourth application, the amplitude in a_j and scatter in c_i decreased by about factor of 2, relative to the first run. As described in § 5.5, this cleaning procedure significantly improves our detection efficiency.

Figure 3 (*left*) shows the rms scatter of the *R*-band light curves for stars on chip 3 with at least 500 data points. The solid curve indicates the photometric precision limit due to Poisson noise of the star and average sky brightness. The internal scatter of the rms distribution in NGC 2158 is somewhat larger than in NGC 6791 (Fig. 3 in Paper III). This is mostly due to the fact that NGC 2158 is a much more centrally concentrated cluster (it has 27% more stars within the central 1′ than does NGC 6791). Most of the stars with higher than average rms at a given magnitude are located at the cluster center. Also, the average seeing for the NGC 2158 data set was inferior to the one for NGC 6791: 2.″3 compared to 2.″1.

Figure 3 (*right*) shows the detection efficiency of 0.95, 1.15, 1.30, and 1.50R_J planets as a function of magnitude and rms scatter (*white*: 0%; *black* 100%), determined in § 5.2.

4.2. *Selection of Transiting Planet Candidates*

For further analysis, we selected stars with at least 500 good epochs, magnitudes $R > 16.29$ (the main-sequence turnoff [MSTO]), and light curve rms below 0.05 mag. This left us with 5159 stars (675, 981, 2680, and 823 stars on chips 1–4, respectively).

To select transiting planet candidates, we used the box-fitting least-squares (BLS) method (Kovács et al. 2002). Adopting a cutoff of 6 in signal detection efficiency (SDE) and 9 in effective signal-to-noise ratio (α), we selected 70 candidates: 3, 21, 17, and 28 on chips 1–4, respectively. Many of the candidates turned out to be known eclipsing binaries; some had sinusoidal light curves or periods that were multiples of a day.

It has been pointed out to us by G. Bákos (2005, private communication) that when the number of transits is small, SDE is not a good statistic. We also examined an additional 102 candidates with SDE < 6 and $\alpha > 20$ (13, 48, 6, and 35 on chips 1–4, respectively). Most of the candidates had very discrepant data on

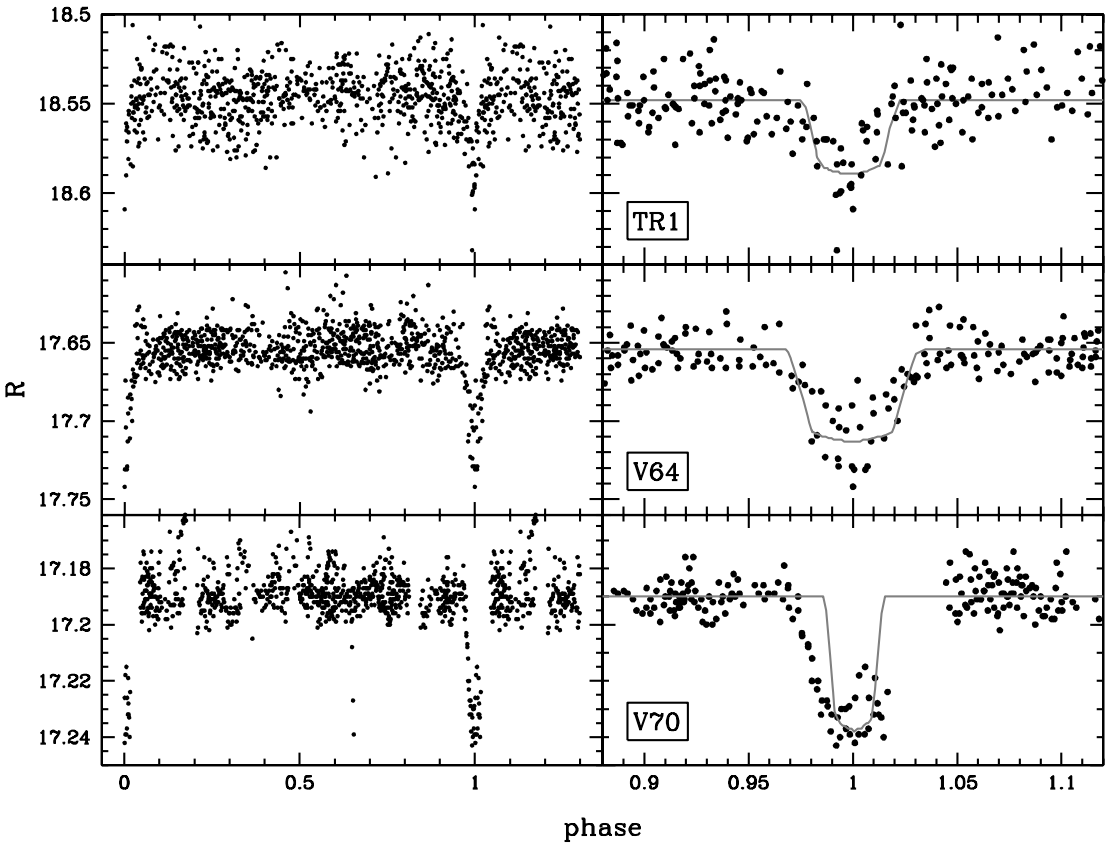

FIG. 4.—*R*-band light curves for three transiting low-luminosity object candidates, TR1 (*top*), V64 (*middle*), and V70 (*bottom*). *Left panels*, Entire phased light curves; *right panels*, close-up of the eclipse, with a simple model superposed (*solid lines*).

one or two nights, most likely due to a nearby saturated star or an unidentified bad column.

4.3. *Candidate Transiting Planets/Low-Luminosity Objects*

We identified one transiting object, TR1, with an *R*-band amplitude of 3.7% and *R*-band magnitude of 18.54. Its *R*-band light curve is shown in Figure 4 (*top left*) and its parameters are listed in Table 1. Using the simple model described in Paper III and § 5.2.1, we find that the light curve is consistent with a 0.87 $R_\odot$ star with a 1.66R_J low-luminosity companion, assuming an orbital inclination of 90°. Figure 4 (*top right*) shows this model (*solid line*) superposed on the *R*-band light curve. It is likely that the star is a cluster member, as it is located 2.′1 from the cluster center, and on the CMD it falls on the cluster MS. The only other possibility is that it is a stellar binary with grazing eclipses.

TABLE 1
LOW-LUMINOSITY TRANSITING OBJECT CANDIDATE IN NGC 2158

Parameter	Value
ID	TR1
$\alpha_{J2000.0}$	06 07 35.4
$\delta_{J2000.0}$	24 05 40.8
P (days)	2.3629
R_{max}	18.544
V_{max}	19.218
A_R	0.037
A_V	...

NOTE.—Units of right ascension are hours, minutes, and seconds, and units of declination are degrees, arcminutes, and arcseconds.

The radii of the seven known Jupiter-mass (0.53M_J–1.45M_J) transiting planets span the range from 1R_J to 1.32R_J (The Extrasolar Planets Encyclopaedia).[4] An eighth planet, HD 149026b, recently found to display transits, has a mass of 0.36M_J and a radius of 0.726R_J (Charbonneau et al. 2006). In light of this, TR1 seems too large to be a planet. Based on models of brown dwarfs (BD) and very low mass stars (VLM), at an age of 1 Gyr a radius of 1.66R_J would correspond to a 0.085 $M_\odot$ star, and at 3.2 Gyr to a 0.140 $M_\odot$ star (Baraffe et al. 2002). Assuming an age of 2 Gyr for NGC 2158, as determined by Ca02, such a radius would correspond to an ∼0.1 $M_\odot$ star. Precise determinations of radii and masses for BDs and VLM stars are few. Until recently, only the nearest such systems could be studied, due to their low luminosities and small radii (hence shallow eclipses). The advent of high-precision mass photometry has stimulated interest in the search for such systems (Hebb et al. 2004; Pont et al. 2005; Pinfield et al. 2005).

Among the candidates with low SDEs, we found two stars, V64 and V70, that exhibit eclipses 4%–5% in depth (Fig. 4). The light curves of V64 and V70 are consistent with 2.4R_J and 2.3R_J objects, respectively, assuming an orbital inclination of 90°. These stars are located above the cluster MS, especially V70 (on chip 4), so they are either blends or field stars.

There are some discrepant points at phase 0.65 in the light curve for V70 that do not seem to be caused by a defect on the

[4] See http://www.obspm.fr/planets.

CCD. It is possible that we have not recovered the correct period for this variable, but more data would be necessary to resolve this issue.

5. ESTIMATE OF THE NUMBER OF EXPECTED DETECTIONS

The number of transiting planets we should expect to find, N_P, can be derived from the following equation:

$$N_P = N_* f_P D, \quad (2)$$

where N_* is the number of stars with sufficient photometric precision, f_P is the frequency of planets within the investigated period range, and D is the detection efficiency, which accounts for random inclinations. In §§ 5.1 and 5.2 we determine f_P and D.

5.1. *Planet Frequency*

The frequency of planets is known to increase with the host star's metallicity. From Figure 7 in Santos et al. (2004), the frequency of planets with metallicities below [Fe/H] = +0.1 dex is ~2.5%. The percentage of planets with periods below 10 days is 15%, as determined in Paper III. Combining these two numbers yields $f_P = 0.375\%$. Please note that the latter estimate is considerably lower than the commonly adopted frequency of 1%.

5.2. *Detection Efficiency*

In order to characterize our detection efficiency, we have inserted model transits into the observed light curves and tried to recover them using the BLS method.

5.2.1. *Model Transit Light Curves*

The model transit light curves were defined by five parameters: the transit depth ΔF, total transit duration t_T, transit duration between ingress and egress t_F (the "flat" part of the transit), period of the planet P, and limb darkening coefficient u. The transit light curves were generated using the approach described in Paper III. To obtain the radius and mass of the cluster stars, we used the $Z = 0.004$, 1.995 Gyr isochrone of Girardi et al. (2000), which is closest to the $Z = 0.0048$, 2 Gyr isochrone used by Ca02. A distance modulus $(m - M)_R = 14.31$ mag was used to bring the observed R-band magnitudes to the absolute magnitude scale (Ca02).

In addition to P, the equations contain two other free parameters: the planet radius, R_P, and the inclination of the orbit, i. A fourth parameter that affects the detectability of a planet is the epoch of the transits, T_0.

5.3. *Test Procedure*

We investigated the range of parameters specified in Table 2, in which P is expressed in days, R_P in R_J, and T_0 as a fraction of the period. We examined the range of periods from 1.05 to 9.85 days and planet radii from $0.95R_J$ to $1.5R_J$, with a resolution of 0.2 days and $0.05R_J$, respectively. For T_0 we used an increment of 5% of the period and a 0.025 increment in cos i. The total number of combinations is 432,000.

TABLE 2
PARAMETER RANGE

Parameter	Minimum	Maximum	Step	n_{steps}
P (days).....	1.05	9.85	0.200	45
R_P/R_J	0.95	1.50	0.050	12
T_0.....	0.00	0.95	0.050	20
cos i	0.0125	0.9875	0.025	40

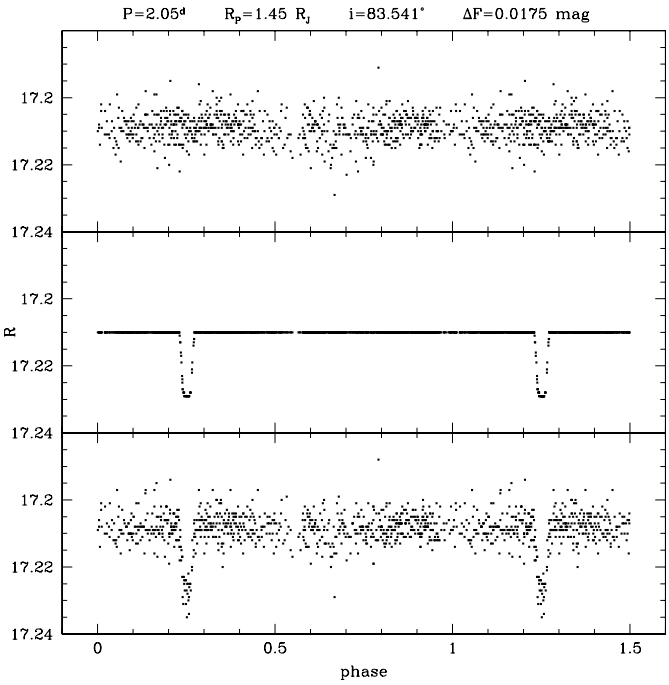

FIG. 5.—Original (*top*), model (*middle*), and combined (*bottom*) light curves for a star with $R = 17.21$ and a planet with a period of 2.05 days, radius of $1.45R_J$, and inclination of 84°.

We followed the test procedure described in Paper III. The tests were run on the 5476 stars from chips 1–4, with at least 500 good epochs and light curve rms below 0.05 mag. Figure 5 shows the original, model, and combined light curves (*top, middle, and bottom panels, respectively*) for a star with $R = 17.21$ and a planet with a period of 2.05 days, radius of $1.45R_J$, and inclination of 84°. The amplitude of the transit is 0.0175 mag, and the mass and radius of the star, taken from the models, are $1.18\,M_\odot$ and $1.10\,R_\odot$.

To assess the impact of the procedure that corrects for offsets between the runs on our detection efficiency, we investigated three cases:

1. Correction applied after inserting transits.
2. Correction applied before inserting transits.
3. Correction was not applied at all.

Case 2 will give us the detection efficiency if our data did not need to be corrected and case 3, if we did not apply the corrections. Case 1 will give us our actual detection efficiency, and its comparison with cases 2 and 3 will show how it is affected by the applied correction procedure.

5.4. *Detection Criteria*

The same detection criteria as in Paper III were used. A transit was flagged as detected if

1. The period recovered by BLS was within 2% of the input period P_{inp}, $2P_{inp}$ or $\frac{1}{2}P_{inp}$.
2. The BLS statistics were above the following thresholds: SDE > 6, $\alpha > 9$.

These detections are referred to hereafter as "firm." Detections where only condition 1 was fulfilled will be called "marginal."

5.5. *Detection Efficiency*

The results of the tests are summarized in Table 3, which lists the test type (1–3), the number and percentage of transits with $t_T \geq 0.5^h$ (out of the 432,000 possible parameter combinations),

TABLE 3
ARTIFICIAL TRANSIT TEST STATISTICS

	All Transits		Model		Marginal		Firm	
Test Type	*N*	Percentage	*N*	Percentage	*N*	Percentage	*N*	Percentage
1.....	40,408	9.4	28,696	71.0	7734	19.1	2818	7.0
2.....	40,408	9.4	28,696	71.0	7493	18.5	2674	6.6
3.....	40,408	9.4	28,696	71.0	4740	11.7	1045	2.6

and the numbers and percentages (relative to the total number of transits in the second column) of transits detected in the model light curves and of marginal and firm detections in the combined light curves.

Figures 6–9 show the dependence of the detection efficiency on period, inclination, planet radius, and transit amplitude. The hatched, open, filled gray, and filled black histograms denote distributions for all transiting planets, planets detected in the model light curves, and marginal and firm detections in the combined light curves, respectively. Left panels show the frequency of transits and transit detections relative to planets with all inclinations. Right panels show the detection completeness normalized to all transiting planets (plotted as hatched histograms in the left panels).

The tests show that 9% of planets with periods 1–10 days will transit their parent stars. This frequency drops from ~22% at $P = 1$ day to ~5% at $P = 10$ days. All planets with inclinations 87°–90° transit their host stars, and this fraction drops to ~78% for $i = 86°$ and ~5% for $i = 79°$. The frequency of transits increases very weakly with planet radius. The distribution of transit amplitudes has a wide peak stretching from 0.8% to 2%, centered on ~1.4%.

The percentage of detections for the model light curves illustrates the limitation imposed on our detection efficiency by the temporal coverage alone. Due to incomplete time sampling, we are restricted to 71% of all planets with periods between 1 and 10 days. For periods below 3 days, our temporal coverage is sufficient to detect ~90% of all transiting planets and drops to ~50% at $P = 7$ days. The detection completeness increases with decreasing inclination, because at lower i, only short-period planets can transit their host stars. It does not depend on the planet radius, and it decreases with increasing transit amplitude.

The source of the dependence of the detection completeness on transit amplitude is not as straightforward as for the other correlations. The amplitude depends on the radii of the star and planet. Since the detection completeness was found to be largely independent of the planet radius, the observed trend must stem from its dependence on the host star's radius, which is a function of its magnitude. Such a correlation is indeed observed, with completeness increasing for brighter stars (not shown here). The link between the temporal coverage and magnitude comes from the observed increase in the number of points in the light curve with decreasing magnitude.

For cases 1, 2, and 3, we *marginally* detect 19%, 19%, and 12% of all transiting planets and *firmly* detect 7.0%, 6.6%, and 2.6%, respectively. Transiting planets with firm detections constitute 80%, 82%, and 80% of all stars with SDE > 6 and $\alpha > 9$. Correcting the light curves after inserting transits (case 1) produces almost the same number of detections, compared to the case in which the correction was applied to the original light curves (case 2). If the light curves were not corrected (case 3), we would detect only 37% of the transiting planets detected in case 1.

The detection completeness for firm detections peaks at 20% for periods of 1–2 days and decreases with period more steeply than in model detections. It does not show a marked dependence

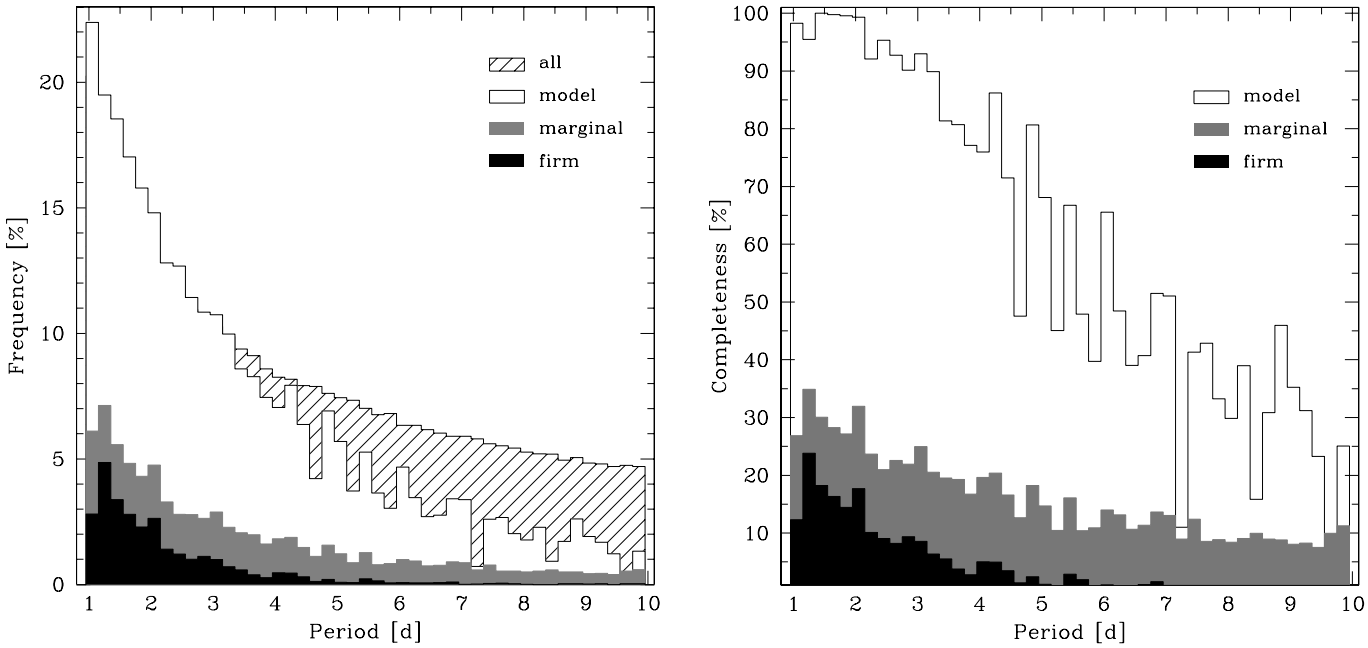

FIG. 6.—Detection efficiency of transiting planets as a function of their period, relative to planets with all inclinations (*left*) and all transiting planets (*right*). Shown are the distributions for all transiting planets (*hatched histogram*), detections in the model light curves (*open histogram*), and marginal (*filled gray histogram*) and firm (*filled black histogram*) detections in the combined light curves.

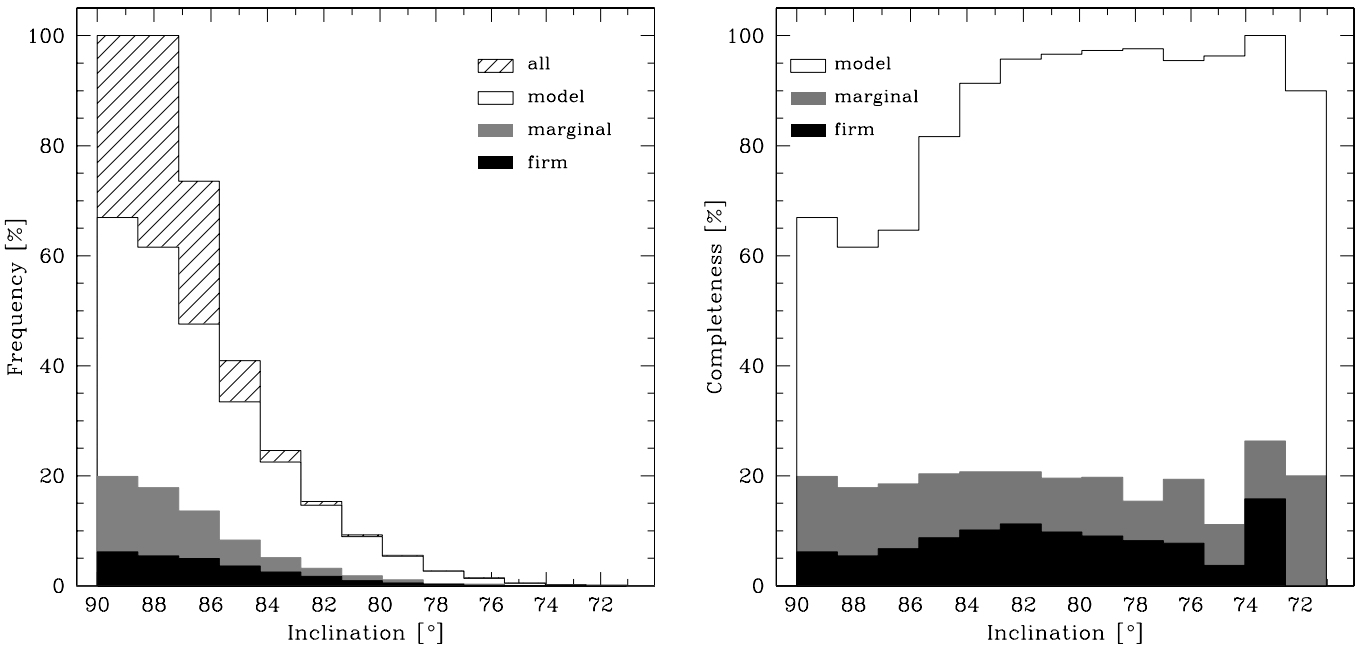

FIG. 7.—Detection efficiency of planetary transits as a function of their inclination, relative to planets with all inclinations (*left*) and all transiting planets (*right*).

on inclination and strongly increases with increasing planet radius, from ∼2% at $1R_J$ to 15% at $1.5R_J$. This is also apparent in Figure 3 (*right*), which shows the detection efficiency of 0.95, 1.15, 1.30, and $1.50R_J$ planets as a function of magnitude and rms scatter (*white*; 0%, *black* 100%).

The detection efficiency peaks at an amplitude of ∼1.5%, due to the most favorable ratio between the transit amplitude and photometric accuracy for this amplitude/magnitude range. The efficiency of *firm* transiting planet detections, relative to planets with all orbital inclinations, D, is 2818/432,000 = 0.65%.

5.6. *Number of Transiting Planets Expected*

In §§ 5.1 and 5.2 we determined the planet frequency f_P to be 0.375%, the number of stars as 5159, and our detection efficiency D as 0.65%. We should therefore expect 0.13 transiting planets among the cluster and field stars.

5.7. *Discussion*

Figure 6 demonstrates that our temporal coverage is not the limiting factor. To increase the number of expected planets, it would be necessary to improve the photometric precision. The weather and seeing conditions turned out to be inferior to what we were expecting. A better quality CCD and a telescope with a larger diameter and/or better observing conditions would be required to improve the chances for a successful transiting planet search in NGC 2158.

The precision of this estimate is largely limited by the uncertainty in one of our basic assumptions, the distribution of planetary

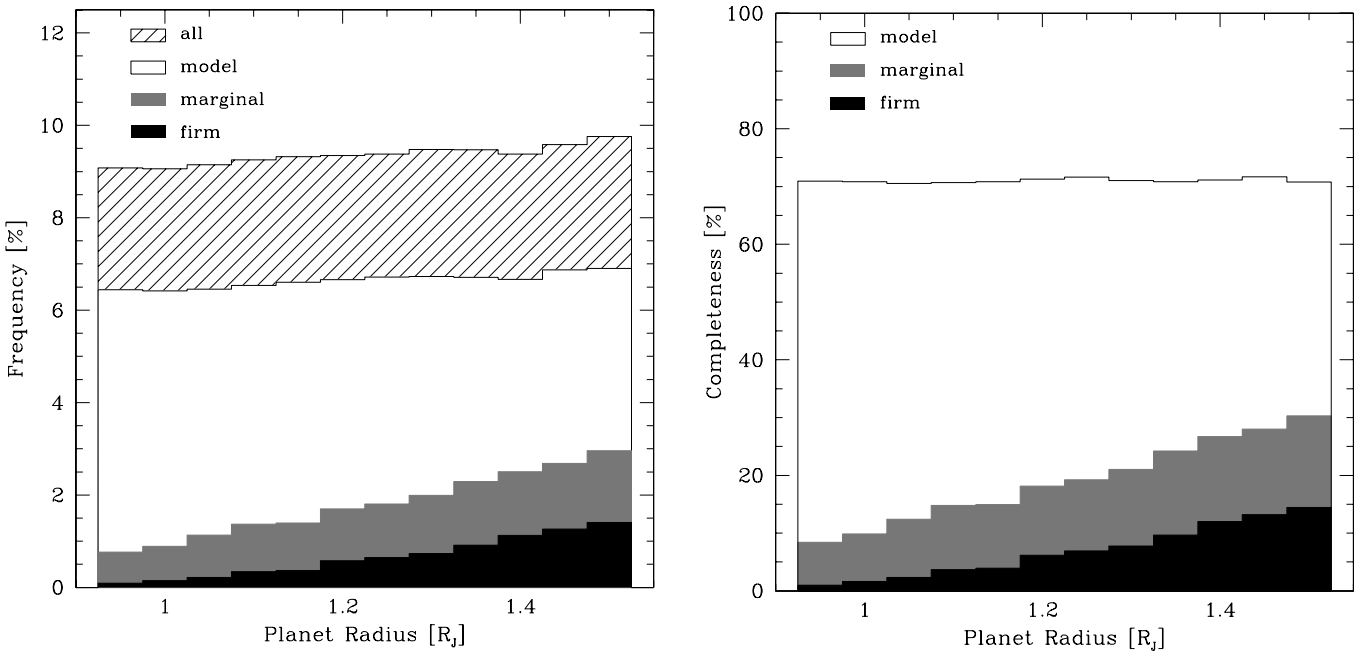

FIG. 8.—Detection efficiency of planetary transits as a function of their radius, relative to planets with all inclinations (*left*) and all transiting planets (*right*).

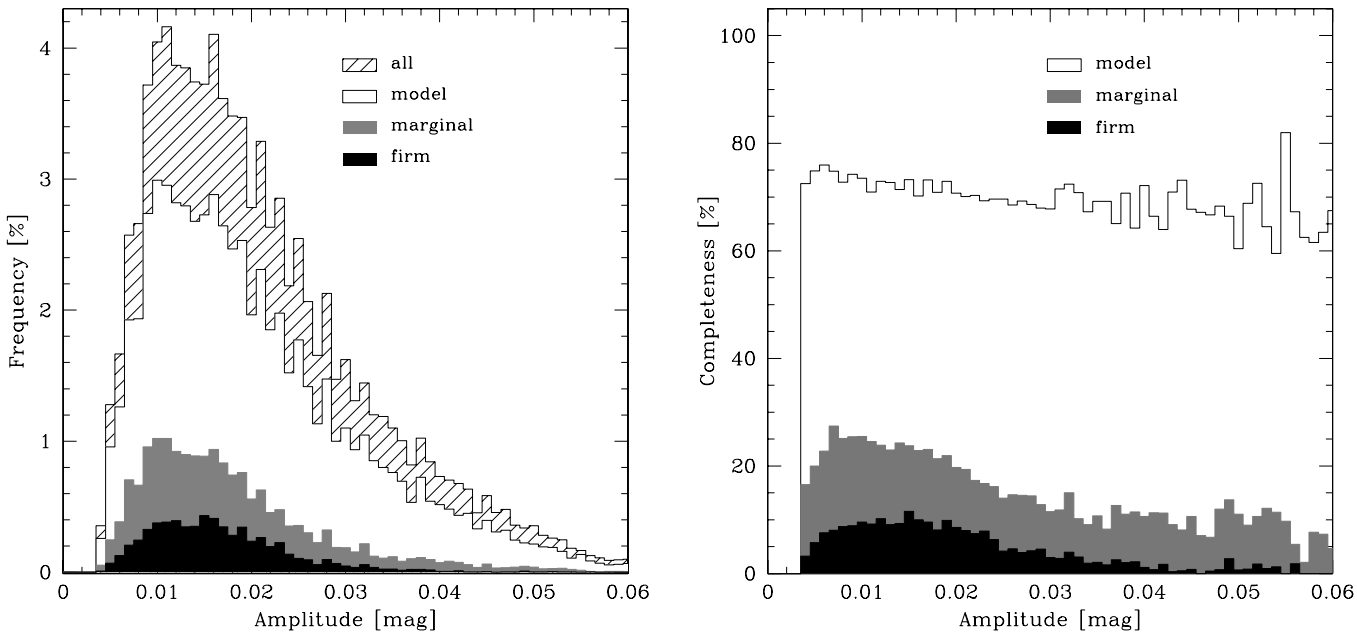

FIG. 9.—Detection efficiency of planetary transits as a function of their amplitude, relative to planets with all inclinations (*left*) and all transiting planets (*right*).

radii. This distribution is not precisely known, and changing it will have a marked effect on the final result. Adopting a distribution of planetary radii from $1.0R_J$ to $1.35R_J$, corresponding to the radius range spanned by the seven known Jupiter-mass transiting planets (The Extrasolar Planets Encyclopaedia) would lower D from 0.65% to 0.33%. This translates to 0.06 detections, compared to 0.13 with the original radius distribution—a 50% decrease.

In Paper I we made the assumption that the planetary radii would span the range $1–3R_J$, based on the radius of $1.347R_J$ for the only known transiting planet at the time, HD 209458b (Brown et al. 2001). A simulation for planets in the radius range $(1.5–3.0)R_J$ shows that 10% of them transit their parent stars, 72% are detected in the model light curves, and 52% and 35% are marginal and firm detections, respectively, in the combined light curves. Assuming that planet radii are distributed evenly between $1R_J$ and $3R_J$ would give the percentage of firm detections as 28% and detection efficiency $D = 2.9\%$, which translates into 0.56 expected detections.

We have detected a star that, if a member of the cluster and not a grazing binary, has a transiting companion with a likely radius of about $1.7R_J$. The detection rate for $1.7R_J$ objects is 21%. This would imply that 0.09% of stars in our field of view have a transiting companion of this mass at close separation (period below 10 days).

6. VARIABLE STARS

We extracted the light curves of 57 known variable stars that were discovered in Paper II. In Tables 4–7 we list their revised parameters.

We searched for new variables by running BLS in the period range 0.1–10 days. We have discovered 40 new variables: 2, 6, 24, and 8 on chips 1–4, respectively: 13 eclipsing binaries, 23 other periodic variables, and four long-period or nonperiodic variables. Their parameters are listed in Tables 4–7, and their light curves are shown in Figures 4 and 10–14.[5] They are also plotted on the CMD in Figure 2.

[5] The *VR* band photometry and finding charts for all variables are available from the authors via anonymous FTP at cfa-ftp.harvard.edu, in the /pub/bmochejs/PISCES directory.

6.1. *Eclipsing Binaries*

There are 13 eclipsing binaries among the newly discovered variables (Figs. 4 and 10, Table 4). V58–V63 are W UMa–type binaries. V60 is very likely a cluster member, based on the KAS97 membership probability and its location on the binary MS. V61 and V63 are located in the blue straggler region. Variables V64 and V67–V70 appear to be detached systems. V64 and V70 were discussed previously in § 4.2. V65 displays continuous variation between the eclipses. It appears to be a cluster member and is located at the base of the red giant branch. The shape of the light curve of V66 changed dramatically between 2003 and 2004. This star is a blue straggler, if it belongs to the cluster.

6.2. *δ Scuti Stars*

In Paper II we reported the discovery of five δ Scuti variables, V35–V39. V71 is a newly discovered variable of this type. We have identified four periods in its light curve. It is located just above the MSTO, together with the other δ Scuti variables (Fig. 2).

Table 5 lists the parameters and Table 6 the periods derived for the δ Scuti variables. Figures 11 and 12 show their light curves phased with every identified period. We have identified at least three modes of pulsation for all variables except V39. The identification of the mode of pulsation in δ Scuti stars is not trivial, as the frequencies of highest amplitude have very different order in different stars (Arentoft et al. 2005). The last two columns of Table 6 give the minimum and maximum difference between the distance modulus computed from the fundamental-mode period-luminosity relation for δ Scuti stars (eq. [4] in Petersen & Christensen-Daalsgard 1999) and the distance modulus $(m - M)_0 = 12.80$ derived by Ca02. These differences are consistent with the variables being members of the cluster, with the exception of V39. It is likely that the discrepancy for this variable is a result of non-fundamental-mode pulsations.

As discussed in Paper II, four of these stars have proper-motion data in KAS97. Cluster membership of V36 is confirmed with high probability, while for V35 and V39 the data are not conclusive. The catalog reports a very low cluster membership probability for V38, which is in disagreement with our conclusions

TABLE 4

ECLIPSING BINARIES IN NGC 2158

ID	$\alpha_{J2000.0}$	$\delta_{J2000.0}$	P (days)	R_{max}	V_{max}	A_R	A_V	P_1 (%)	P_2 (%)
V01	06 07 32.6	23 49 21.0	0.2353	17.659	18.497	0.080	0.117	...	...
V58	06 07 47.8	23 51 16.0	0.2553	19.870	20.547	0.291	0.454	...	...
V59	06 07 23.9	24 04 57.5	0.3144	16.430	16.932	0.055	0.056	...	...
V02	06 07 23.3	24 06 12.3	0.3385	17.340	17.872	0.240	0.241	...	...
V60	06 07 38.0	24 07 24.9	0.3413	16.972	17.564	0.238	0.269	63	77
V03	06 07 04.9	23 48 53.3	0.3522	18.396	18.993	0.680	0.737	...	...
V04	06 07 17.5	24 04 45.7	0.3555	17.749	18.376	0.219	0.269	...	...
V05	06 07 40.6	24 05 03.6	0.3635	17.623	18.197	0.395	0.416	...	...
V61	06 06 48.3	23 52 44.0	0.3914	15.144	15.542	0.195	0.184	...	...
V07	06 06 37.0	23 50 41.1	0.5075	17.043	17.543	0.037	0.058	...	...
V08	06 06 44.8	24 06 57.8	0.5466	17.632	18.561	0.075	0.164	...	...
V09	06 07 29.4	24 10 06.3	0.6793	18.852	19.502	0.686	0.680	...	...
V10	06 07 34.9	24 04 25.6	0.8602	18.740	19.416	0.346	0.370	...	...
V17	06 07 31.9	24 06 00.2	0.8633	15.682	16.173	0.025	0.039	...	...
V62	06 07 32.8	24 07 26.6	0.8706	17.202	17.742	0.046	0.069	...	...
V11	06 07 21.4	24 05 39.7	0.9105	17.066	17.627	0.155	0.139	...	...
V19	06 06 20.5	24 04 47.8	0.9661	17.414	18.388	0.066	0.110	...	...
V12	06 07 18.7	24 06 50.0	1.0573	16.610	17.138	0.043	0.052	71	78
V63	06 07 37.5	23 55 57.3	1.0819	15.111	15.368	0.016	0.018	8	43
V13	06 07 28.1	24 06 35.3	1.2033	15.882	16.374	0.086	0.084	...	...
V14	06 07 27.2	23 52 24.4	1.2095	16.544	17.198	0.100	0.124	1	28
V15	06 07 36.1	23 48 24.0	1.5588	16.088	16.439	0.028	0.039	...	...
V16	06 06 36.6	24 03 29.1	1.5898	17.742	18.355	0.057	0.100	...	...
V64	06 07 17.8	24 05 32.5	1.7960	17.651	18.314	0.053	...	...	...
V65	06 07 39.3	24 02 16.0	1.8356	15.426	15.944	0.026	0.030	60	82
V18	06 07 31.0	24 05 50.4	1.9013	16.534	16.994	0.043	0.051	...	...
V66	06 07 31.4	24 05 18.4	2.0214	15.243	15.533	0.060	0.044	...	...
V20	06 07 20.6	24 06 01.2	2.0611	16.420	16.947	0.100	0.111	...	...
V21	06 07 36.3	23 56 21.3	2.0638	16.777	17.195	0.039	0.049	10	47
V22	06 07 37.7	24 07 40.2	2.1307	15.243	15.762	0.016	0.021	72	90
V23	06 07 03.5	24 01 45.1	2.2597	18.290	19.289	0.137	0.224	...	...
V24	06 07 43.4	24 06 22.8	2.3002	16.718	17.217	0.043	0.063	59	79
V67	06 07 24.1	24 06 22.7	2.3370	17.586	18.084	0.206	0.204	...	...
V25	06 07 19.9	24 06 24.4	2.3677	16.358	16.842	0.038	0.042	...	...
V68	06 07 27.6	24 10 48.8	2.4795	18.439	19.054	0.259	0.366	...	...
V27	06 07 30.2	24 07 50.5	2.4954	16.827	17.283	0.043	0.076	...	...
V26	06 07 24.1	24 07 53.8	2.6735	16.808	17.299	0.047	0.085	...	...
V34	06 07 19.9	23 49 51.4	2.8640	15.789	15.989	0.150	0.164	...	...
V28	06 06 50.0	24 08 26.0	2.9255	17.290	17.912	0.154	0.166	15	59
V29	06 06 46.2	23 49 41.3	3.1572	18.457	19.028	0.451	0.456	...	...
V30	06 07 14.9	24 09 40.8	3.3461	18.924	19.572	0.361	0.312	...	...
V69	06 07 22.2	24 06 15.4	3.7788	16.202	16.640	0.164	0.185	...	...
V31	06 06 49.0	24 01 43.7	3.7833	15.970	16.696	0.066	0.067	11	47
V32	06 07 27.9	24 06 22.7	4.5948	16.458	16.984	0.183	0.048	...	...
V33	06 07 33.3	24 04 34.4	4.7397	16.415	16.902	0.030	0.049	...	...
V70	06 06 36.9	24 02 05.9	6.2657	17.189	17.910	0.043	...	...	...
V55	06 07 25.8	24 05 45.7	8.1563	15.616	16.192	0.143	0.197	...	...

NOTES.—Units of right ascension are hours, minutes, and seconds, and units of declination are degrees, arcminutes, and arcseconds. Cluster core and corona membership probabilities P_1 and P_2 are taken from KAS97.

TABLE 5
OTHER PERIODIC VARIABLES IN NGC 2158

ID	$\alpha_{J2000.0}$	$\delta_{J2000.0}$	P (days)	$\langle R \rangle$	$\langle V \rangle$	A_R	A_V	P_1 (%)	P_2 (%)
V35	06 06 47.1	24 07 41.5	0.0981	15.820	16.351	0.008	0.014	13	58
V36	06 07 16.8	24 05 44.9	0.1078	15.987	16.473	0.022	0.033	83	90
V71	06 07 23.8	24 10 40.4	0.1112	16.210	16.675	0.003	0.005	...	...
V37	06 07 26.0	24 04 23.6	0.1113	15.794	16.236	0.037	0.048	...	...
V38	06 07 11.3	24 03 36.4	0.1205	15.619	16.053	0.005	0.007	3	4
V39	06 06 50.6	24 10 56.5	0.1220	15.211	15.648	0.018	0.024	4	23
V72	06 06 11.4	24 08 52.9	0.3084	18.187	19.282	0.020	0.021	...	...
V73	06 06 50.6	24 09 58.3	0.3729	18.383	19.549	0.020	0.019	...	...
V74	06 06 27.9	24 03 47.4	0.6762	19.560	20.687	0.064	0.053	...	...
V75	06 06 32.1	24 08 51.5	0.6778	15.844	16.195	0.003	0.003	2	37
V76	06 07 23.1	24 10 00.5	0.7981	16.787	17.263	0.005	0.005	54	79
V77	06 07 25.4	24 09 21.6	1.1442	16.657	17.116	0.007	0.008	...	...
V78	06 07 37.6	24 05 57.3	1.2027	16.786	17.277	0.004	0.005	...	...
V79	06 07 42.2	23 50 39.0	1.3118	18.337	19.026	0.028	0.028	...	...
V40	06 07 05.6	24 07 06.5	1.3592	18.178	19.033	0.018	0.022	...	...
V80	06 07 32.5	24 10 09.7	1.4727	16.799	17.229	0.007	0.009	...	...
V41	06 07 04.2	23 58 09.5	1.4949	17.079	17.795	0.026	0.030	7	28
V42	06 07 36.3	24 02 07.4	1.6210	17.425	17.911	0.031	0.037	67	88
V43	06 07 49.9	24 09 45.5	2.6060	16.588	17.056	0.008	0.007	...	...
V44	06 07 05.8	24 08 51.3	2.8294	16.684	17.391	0.016	0.021	44	80
V81	06 07 40.6	24 05 50.0	2.9942	15.891	16.196	0.011	0.009	19	23
V45	06 06 27.8	23 49 58.6	5.0129	18.937	19.845	0.036	0.050	...	...
V82	06 06 24.2	24 06 43.5	5.3317	15.476	16.109	0.003	0.004	...	...
V46	06 07 09.7	24 06 50.2	5.4488	17.378	18.153	0.014	0.024	...	...
V47	06 06 40.4	24 06 34.3	5.4962	17.255	17.931	0.009	0.011	7	51
V83	06 07 49.4	24 09 13.2	5.8010	15.529	16.050	0.009	0.012	...	...
V54	06 07 07.0	24 05 25.3	6.3310	15.373	15.891	0.009	0.009	...	...
V48	06 07 06.2	24 02 10.1	6.4713	16.422	17.115	0.025	0.031	41	69
V49	06 07 10.2	24 10 19.4	6.5614	16.520	17.231	0.024	0.032	26	51
V84	06 07 31.8	23 48 28.9	7.0849	17.284	18.303	0.010	0.015	...	...
V85	06 06 22.3	24 07 09.1	7.2146	15.630	16.295	0.005	0.006	...	...
V50	06 06 43.0	23 55 15.1	7.8975	16.266	16.803	0.011	0.014	0	24
V86	06 07 22.7	23 48 19.0	9.1927	17.706	18.749	0.020	0.028	...	...
V87	06 06 43.9	23 54 04.9	9.3788	16.509	16.953	0.006	0.012	...	...
V53	06 07 49.0	24 02 02.6	9.8949	17.023	17.849	0.014	0.016	34	65
V88	06 07 47.5	24 04 42.4	9.9873	16.907	17.715	0.008	0.010	25	38
V89	06 07 36.4	24 05 42.3	12.5495	15.673	16.299	0.008	0.008	...	...
V90	06 07 36.2	24 05 25.4	12.8136	15.924	16.580	0.005	0.008	...	...
V52	06 06 24.0	23 54 25.6	16.0765	16.062	16.523	0.007	0.012	...	...
V91	06 07 35.2	23 50 38.2	20.7403	17.337	18.007	0.009	0.008	...	...
V92	06 07 24.7	24 03 58.9	30.4984	16.333	17.075	0.011	0.014	...	...
V93	06 06 36.3	24 04 17.9	36.8876	17.759	19.219	0.040	0.060	...	...
V56	06 06 17.2	24 03 39.7	63.4571	16.746	17.305	0.029	0.016	...	...

NOTES.—Units of right ascension are hours, minutes, and seconds, and units of declination are degrees, arcminutes, and arcseconds. Cluster core and corona membership probabilities P_1 and P_2 are taken from KAS97.

TABLE 6
PROPERTIES OF δ SCUTI STARS IN NGC 2158

ID	P_1 (days)	P_2 (days)	P_3 (days)	P_4 (days)	P_5 (days)	P_6 (days)	$\Delta(m-M)_0^{\min}$	$\Delta(m-M)_0^{\max}$
V35.....	0.098051	0.104421	0.090706	0.084631	0.114466	0.084468	-0.055	-0.398
V36.....	0.107822	0.111340	0.114872	...	...	...	0.119	0.221
V37.....	0.111281	0.106033	0.113535	...	...	...	-0.035	-0.145
V38.....	0.120463	0.074820	0.080215	...	...	...	-0.122	-0.892
V39.....	0.121997	...	...	...	...	...	-0.506	-0.506
V71.....	0.111217	0.097834	0.084016	0.088923	...	...	0.009	0.371

based on the δ Scuti *P-L* relation. The study of KAS97 was also targeting much brighter stars ($V > 8$ mag) in M35 and two other clusters at smaller distances than NGC 2158. The authors say that their proper motion measurement "accuracy decreases rapidly for stars fainter than $V = 15.5$ mag," while the V magnitude range of NGC 2158 variables is 15.7–18.0, and $V = 16.04$ for V38.

6.3. *Other Periodic Variables*

We have discovered 22 new other periodic variables (Fig. 13, Table 5). They display roughly sinusoidal light variations with periods ranging from 0.3 to 36 days. The variability in most of these stars is probably caused by starspots, which are rotating in and out of view. Variables V83, V84, V88, and V89, in addition to periodic variability, show a change in the magnitude zero point between the 2003 and 2004 observations, which is most likely caused by the evolution of starspots.

On the CMD, V75 and V81 are located in the blue straggler region of the CMD; V76, V77, V78, V80, and V87 are located close to MSTO; and V82, V83, V85, and V89 are located near the subgiant branch (SGB). The variable V90, if it belongs to the cluster, might be a member of the newly proposed class of variable stars termed "red stragglers" (Albrow et al. 2001) or "sub-subgiant stars" (Mathieu et al. 2003). Thus far, the origin and evolutionary status of these stars remains unknown. V79 and V91 are located above the MS and may be binary stars or background objects, and V72, V73, V74, V84, V86, V88, and V92 seem to be background objects. According to KAS97, V76 is most likely a cluster member, and for V75, V81, and V88, the data are not conclusive.

6.4. *Cataclysmic Variable Candidate*

In Figure 14 we present the light curve of the cataclysmic variable candidate V57, identified in Paper II. The variable shows four 2.5 mag outbursts that phase with a 48.2 day period (phased light curve shown in Fig. 13).

In Paper II we determined the $V - R$ color of this variable to be -0.26 at maximum and -0.31 at minimum. In our current data the variable has a much more plausible $V - R$ color: 0.304 at maximum and 0.874 at minimum. The color determination at minimum is very uncertain due to the faintness of the star and differing minimum magnitudes between the cycles.

Assuming the NGC 2158 distance and reddening derived by Ca02, we get the minimum absolute V-band magnitude M_V(min) of 6.4 mag. From Figure 3.5 in Warner (1995) it is apparent that M_V(min) is roughly 8 mag for U Gem–type dwarf novae, but even the most extreme Z Cam–type systems have M_V(min) > 6.8 mag. This would imply that V57 is a dwarf nova located in front of the cluster.

It should be noted, however, that the V-band magnitude alone is not sufficient to exclude this variable as a cluster member. Another cataclysmic variable, B7 in the open cluster NGC 6791, is seen most of the time in a high state at $M_V \sim 5$ and has been caught only once in its low state at M_V(min) = 7.4 (Kaluzny et al. 1997). The high state in VY Scl-type cataclysmic variables can last for several years, and some systems stay in the high state most of the time (i.e., ST LMi, MR Ser, and AN UMa; Kafka & Honeycutt 2005). Further investigation is needed to resolve the nature of V57. A spectrum of a dwarf nova in quiescence should display Balmer emission on a blue continuum. During outburst the emission lines are gradually overwhelmed by the increasing continuum and development of broad absorption lines (Warner 1995). If V57 is in a "high" level, like B7, then this will be apparent in the spectrum, and emission lines should not be prominent.

6.5. *Long-Period and Nonperiodic Variables*

We have discovered four new long-period or nonperiodic variables (Fig. 14, Table 7). V94 is located near the SGB. V95 is located in the red straggler region of the CMD. According to KAS97, V95 is likely a cluster member. V96 and V97 are located on the upper MS, close to the MSTO. V96 is a detached

TABLE 7
MISCELLANEOUS VARIABLES IN NGC 2158

ID	$\alpha_{J2000.0}$	$\delta_{J2000.0}$	$R_{\max}$	$V_{\max}$	A_R	A_V	P_1 (%)	P_2 (%)
V57.....	06 07 33.8	24 07 55.2	18.322	18.626	3.495	4.317	...	...
V94.....	06 07 27.2	24 04 35.5	15.408	16.197	0.057	0.066	...	...
V95.....	06 07 18.8	24 01 40.1	15.922	16.703	0.039	0.045	53	70
V96.....	06 07 32.0	24 06 33.7	16.363	16.865	0.139	0.149	...	...
V97.....	06 07 17.3	24 02 46.5	16.824	17.350	0.116	0.142	...	...

NOTE.—Units of right ascension are hours, minutes, and seconds, and units of declination are degrees, arcminutes, and arcseconds.

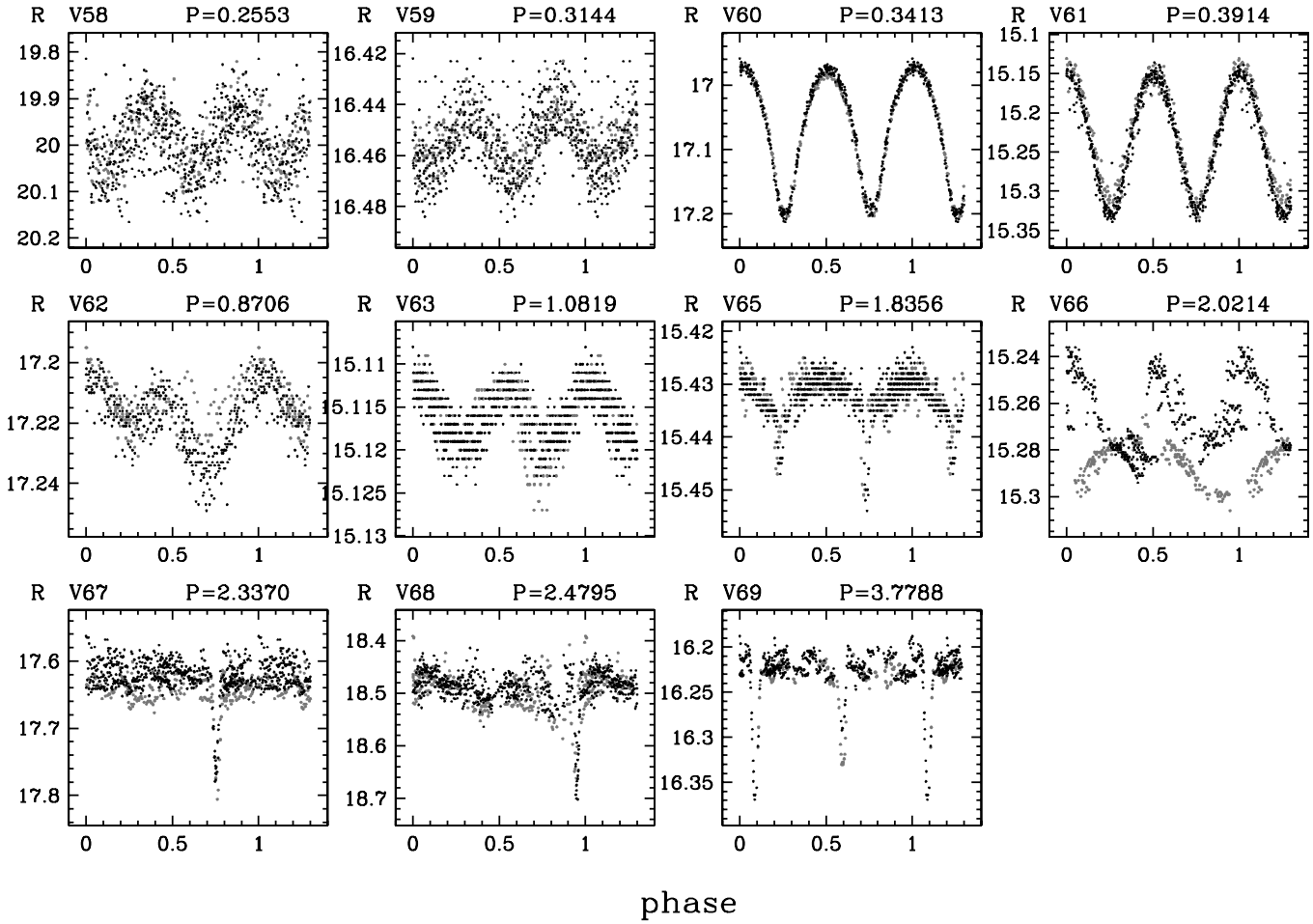

FIG. 10.—*R*-band light curves of 11 new eclipsing binaries. Data points from the first observing season are denoted by gray symbols and from the second season by black symbols.

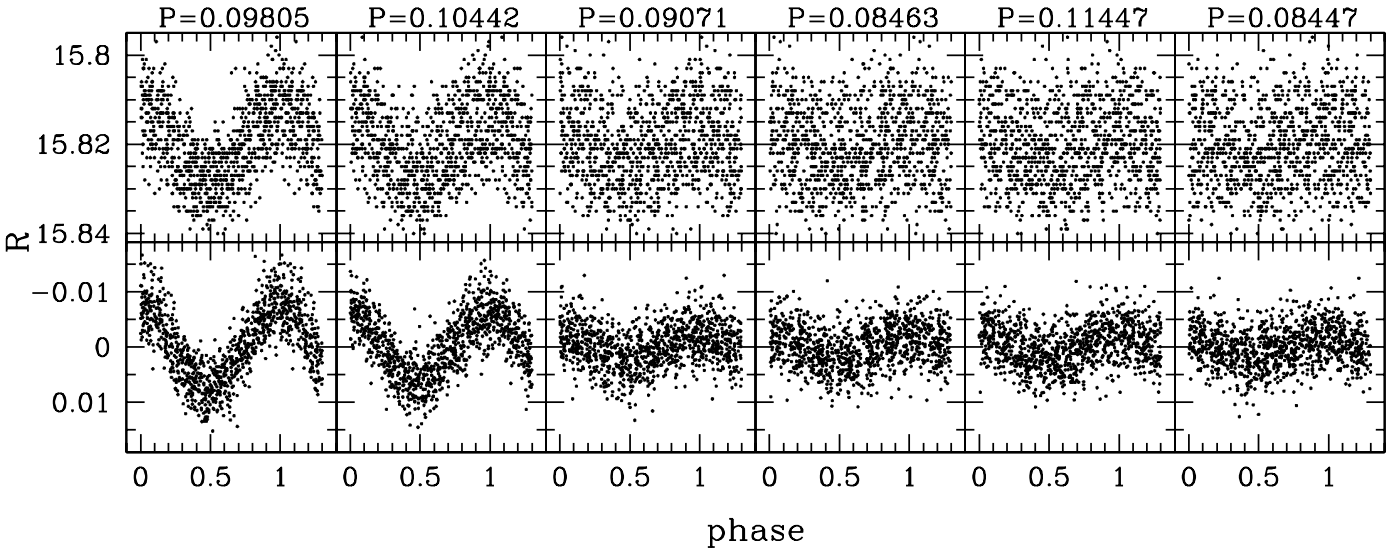

FIG. 11.—*R*-band light curves of δ Scuti variable V35, phased with each of the six detected periods. *Top panels*, Raw; *bottom panels*, subtracted of variability corresponding to other periods.

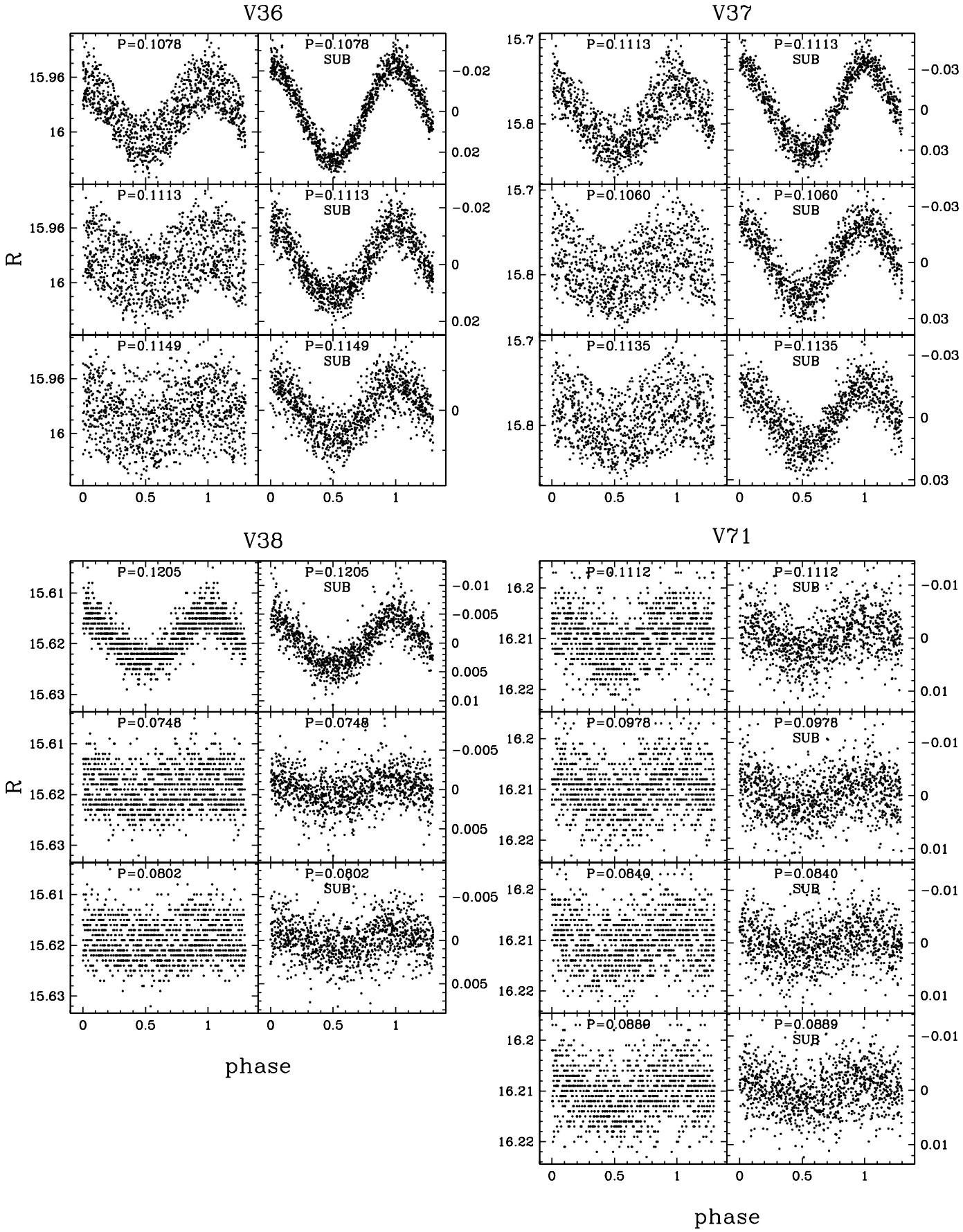

FIG. 12.—*R*-band light curves of δ Scuti variables V36, V37, V38, and V71, phased with each detected period. *Left panels*, Raw; *right panels*, subtracted of variability corresponding to other periods.

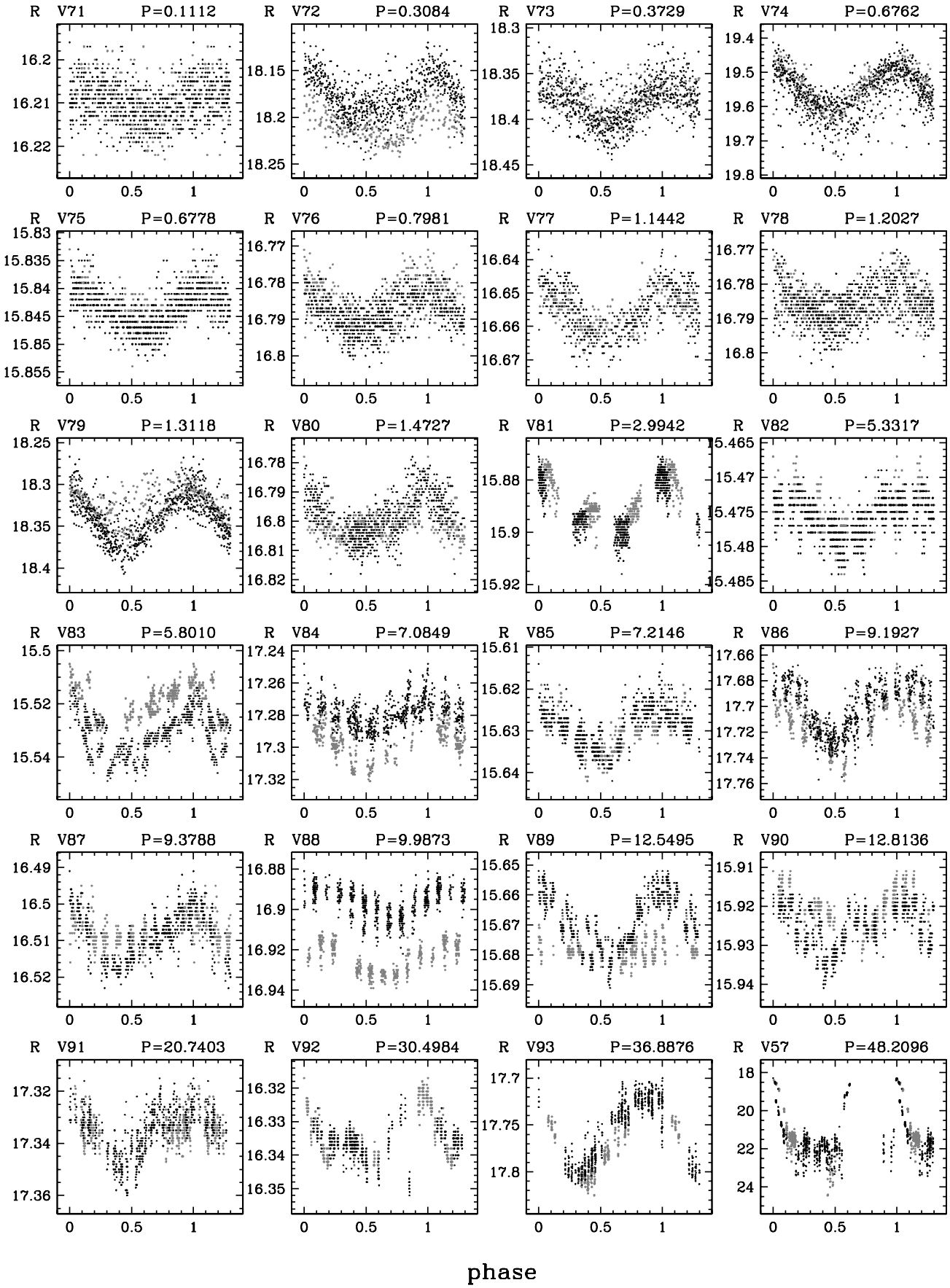

FIG. 13.—*R*-band light curves of 23 new periodic variables and the light curve of the cataclysmic variable V57 phased with the proposed cycle length of 48.2 days. Data points from the first observing season are denoted by gray symbols and from the second season by black symbols.

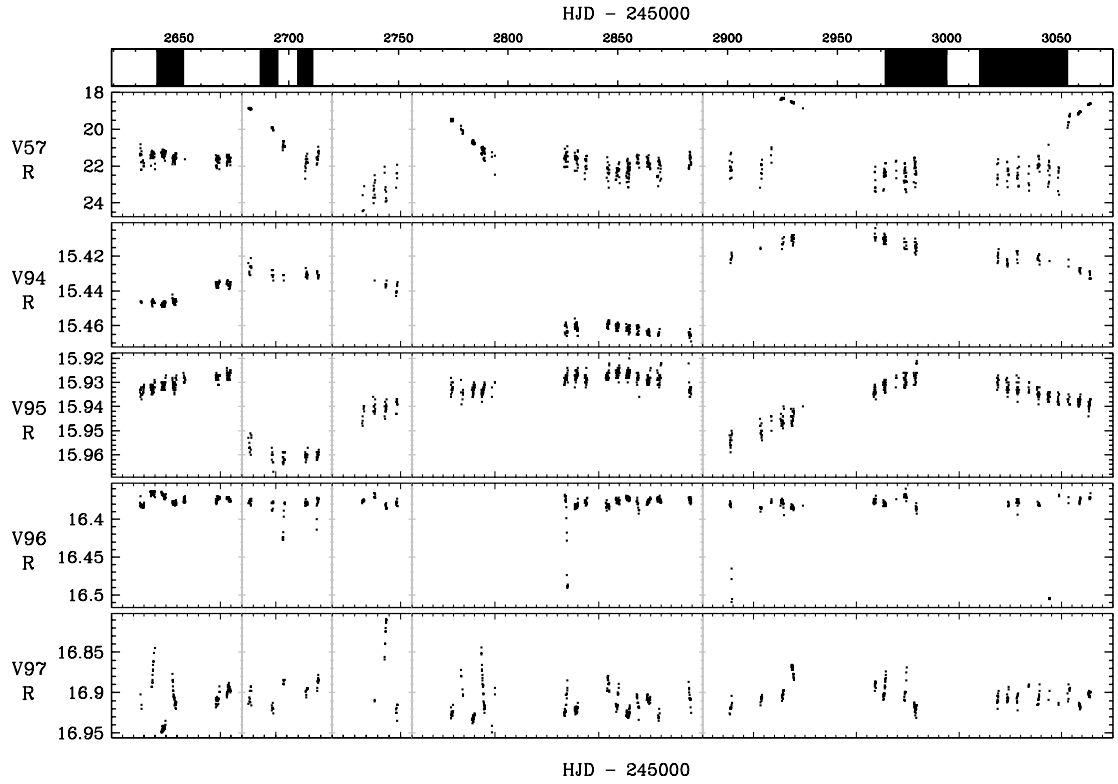

FIG. 14.—*R*-band light curves of miscellaneous variables. The top panel illustrates the distribution in time of the five subwindows plotted for the variables.

eclipsing binary and could be useful for cluster distance and age determination, due to its location on the MSTO.

7. CONCLUSIONS

In this paper we have performed an extensive search for transiting planets in the intermediate-age, populous cluster NGC 2158. The cluster was monitored for over 260 hr during 59 nights.

We have identified a low-luminosity transiting object candidate, TR1. The *R*-band amplitude of 3.7% implies a $1.66R_J$ radius for the transiting companion. The location of the host star on the cluster MS and its proximity to the cluster center seem to indicate that it is a member of the cluster. Higher accuracy light curves are required to better constrain the radius and period of TR1, and follow-up spectroscopy is required to estimate the mass of the transiting object through a measurement or an upper limit on the central object's radial velocity variations.

Assuming a planet frequency from radial velocity surveys, we estimate that we should have detected 0.13 transiting planets with periods between 1 and 10 days, with our photometric precision and temporal coverage. The main limitation on our detection efficiency was imposed by the photometric precision.

We have discovered 40 new variable stars in NGC 2158: 13 eclipsing binaries, 23 other periodic variables, and four nonperiodic variables. Together with 57 variables discovered in Paper II, this brings the total number of known variables in this cluster to 97. We have also presented high photometric precision light curves, spanning almost 13 months, for all previously known variables.

Transiting planets have proven to be more challenging to detect than initially expected, as shown by the paucity of detections from the many searches underway in open clusters (i.e., Bruntt et al. 2003; UStAPS: Hood et al. 2005; EXPLORE/OC: von Braun et al. 2004; STEPSS: Marshall et al. 2005) and in the Galactic field (i.e., EXPLORE: Mallén-Ornelas et al. 2003; Optical Gravitational Lensing Experiment : Udalski et al. 2002c; STARE: Alonso et al. 2003; Hungarian Automated Telescope: Bakos et al. 2004; WASP0: Kane et al. 2005).[6] To date, only six planets have been discovered independently by transit searches, all of them in the field, and five of those were initially identified by OGLE (Udalski et al. 2002a, 2002b, 2002c, 2003; Alonso et al. 2004).

We would like to thank the FLWO 1.2 m Time Allocation Committee for the generous amount of time we were allocated for this project. This publication makes use of data products from: the Two Micron All Sky Survey, which is a joint project of the University of Massachusetts and the Infrared Processing and Analysis Center/California Institute of Technology, funded by the National Aeronautics and Space Administration and the National Science Foundation; the Digital Sky Survey, produced at the Space Telescope Science Institute under US Government grant NAGW-2166; the SIMBAD database, operated at CDS, Strasbourg, France; and the WEBDA open cluster database maintained by J. C. Mermilliod (http://obswww.unige.ch/webda/).

Support for B. J. M. and J. N. W. was provided by NASA through Hubble Fellowship grants HST-HF-01155.02-A and HST-HF-01180.01-A from the Space Telescope Science Institute, which is operated by the Association of Universities for Research in Astronomy, Inc., under NASA contract NAS5-26555. K. Z. S. acknowledges support from the William F. Milton Fund.

[6] For a more complete list of transiting planet searches, please refer to http://star-www.st-and.ac.uk/~kdh1/transits/table.html and http://www.obspm.fr/encycl/searches.html.

REFERENCES

Alard, C. 2000, A&AS, 144, 363
Alard, C., & Lupton, R. 1998, ApJ, 503, 325
Albrow, M. D., Gilliland, R. L., Brown, T. M., Edmonds, P. D., Guhathakurta, P., & Sarajedini, A. 2001, ApJ, 559, 1060
Alonso, R., Belmonte, J. A., & Brown, T. 2003, Ap&SS, 284, 13
Alonso, R., et al. 2004, ApJ, 613, L153
Arentoft, T., Bouzid, M. Y., Sterken, C., Freyhammer, L. M., & Frandsen, S. 2005, PASP, 117, 601
Bakos, G., Noyes, R. W., Kovács, G., Stanek, K. Z., Sasselov, D. D., & Domsa, I. 2004, PASP, 116, 266
Baraffe, I., Chabrier, G., Allard, F., & Hauschildt, P. H. 2002, A&A, 382, 563
Brown, T. M., Charbonneau, D., Gilliland, R. L., Noyes, R. W., & Burrows, A. 2001, ApJ, 552, 699
Bruntt, H., Grundahl, F., Tingley, B., Frandsen, S., Stetson, P. B., & Thomsen, B. 2003, A&A, 410, 323
Carraro, G., Girardi, L., & Marigo, P. 2002, MNRAS, 332, 705 (Ca02)
Charbonneau, D., et al. 2006, ApJ, 636, 445
Christian, C. A., Heasley, J. N., & Janes, K. A. 1985, ApJ, 299, 683
Cutri, R. M., et al. 2003, The 2MASS All-Sky Catalog of Point Sources (Pasadena: IPAC)
Girardi, L., Bressan, A., Bertelli, G., & Chiosi, C. 2000, A&AS, 141, 371
Hebb, L., Wyse, R. F. G., & Gilmore, G. 2004, AJ, 128, 2881
Hood, B., et al. 2005, MNRAS, 360, 791
Kafka, S., & Honeycutt, R. K. 2005, AJ, 130, 742
Kaluzny, J., Stanek, K. Z., Garnavich, P. M., & Challis, P. 1997, ApJ, 491, 153
Kane, S. R., Lister, T. A., Collier Cameron, A., Horne, K., James, D., Pollacco, D. L., Street, R. A., & Tsapras, Y. 2005, MNRAS, 362, 117
Kharchenko, N., Andruk, V., & Schilbach, E. 1997, Astron. Nachr., 318, 253 (KAS97)
Konacki, M., Torres, G., Jha, S., & Sasselov, D. D. 2003, Nature, 421, 507
Kovács, G., Zucker, S., & Mazeh, T. 2002, A&A, 391, 369
Mallén-Ornelas, G., Seager, S., Yee, H. K. C., Minniti, D., Gladders, M. D., Mallén-Fullerton, G. M., & Brown, T. M. 2003, ApJ, 582, 1123
Marshall, J. L., Burke, C. J., DePoy, D. L., Gould, A., & Kollmeier, J. A. 2005, AJ, 130, 1916
Mathieu, R. D., van den Berg, M., Torres, G., Latham, D., Verbunt, F., & Stassun, K. 2003, AJ, 125, 246
Mochejska, B. J., Stanek, K. Z., Sasselov, D. D., & Szentgyorgyi, A. H. 2002, AJ, 123, 3460 (Paper I)
Mochejska, B. J., Stanek, K. Z., Sasselov, D. D., Szentgyorgyi, A. H., Westover, M., & Winn, J. N. 2004, AJ, 128, 312 (Paper II)
Mochejska, B. J., et al. 2005, AJ, 129, 2856 (Paper III)
Petersen, J. O., & Christensen-Dalsgaard, J. 1999, A&A, 352, 547
Pinfield, D. J., Jones, H. R. A., & Steele, I. A. 2005, PASP, 117, 173
Pont, F., Melo, C. H. F., Bouchy, F., Udry, S., Queloz, D., Mayor, M., & Santos, N. C. 2005, A&A, 433, L21
Santos, N. C., Israelian, G., & Mayor, M. 2004, A&A, 415, 1153
Stetson, P. B. 1987, PASP, 99, 191
Tamuz, O., Mazeh, T., & Zucker, S. 2005, MNRAS, 356, 1466
Udalski, A., Pietrzynski, G., Szymanski, M., Kubiak, M., Zebrun, K., Soszynski, I., Szewczyk, O., & Wyrzykowski, L. 2003, Acta Astron., 53, 133
Udalski, A., Szewczyk, O., Zebrun, K., Pietrzynski, G., Szymanski, M., Kubiak, M., Soszynski, I., & Wyrzykowski, L. 2002a, Acta Astron., 52, 317
Udalski, A., Zebrun, K., Szymanski, M., Kubiak, M., Soszynski, I., Szewczyk, O., Wyrzykowski, L., & Pietrzynski, G. 2002b, Acta Astron., 52, 115
Udalski, A., et al. 2002c, Acta Astron., 52, 1
von Braun, K., Lee, B. L., Mallén-Ornelas, G., Yee, H. K. C., Seager, S., & Gladders, M. D. 2004, in AIP Conf. Proc. 713, The Search for Other Worlds, ed. S. S. Holt & D. Deming (New York: AIP), 181
Warner, B. 1995, Cataclysmic Variable Stars (New York: Cambridge Univ. Press)